Proceedings of the 1996 IEEE
International Conference on Robotics and Automation
Minneapolis, Minnesota - April 1996

The Noise Amplification Index for Optimal Pose Selection in Robot Calibration

Ali Nahvi and John M. Hollerbach

Depts. Mechanical Engineering and Computer Science
Univ. Utah, Salt Lake City, UT 84112

Abstract

This paper presents a new observability index to quantify the selection of best pose set in robot calibration. This noise amplification index is considerably more sensitive to calibration error than previously published observability indices. Support for the proposed index is provided analytically and geometrically, and also through comparison against previous indices by a simulation for a 3-link planar robot and by an experiment for a 3-DOF redundant parallel-drive robot.

1 Introduction

To implement calibration by kinematic loop methods [6], a robot should be placed into poses that result in the most accurate estimates. For some poses, the parameters of the robot do not influence the sensor measurements much: the effects of noise and of unmodeled sources of error dominate the effect of length and other kinematic parameter variations of the robot. As a result, the calibrated parameters obtained will not be reliable.

Investigators have proposed a variety of observability indices to quantify the goodness of pose selection; these indices are based on the singular value decomposition (SVD) of the Jacobian matrix of the differential kinematics [9]. Menq and Borm [8] proposed an observability index related to the product of all singular values. Driels and Pathre [3] proposed the condition number; Schroer et al. [11] stated that a condition number below 100 is required for reliable results. Nahvi et al. [10] proposed the minimum singular value. In this paper, we present a new observability index, termed the *noise amplification index,* which is the ratio of maximum singular value to condition number, as the best criterion for pose selection. Formal arguments for the noise amplification index are given, and simulation and experimental comparisons relative to the other indices are given.

For a reliable observability index, it is first necessary to perform task variable and parameter scalings to make the singular values comparable [5, 6, 11]. If a proper scaling is not implemented, the comparison of the singular values will be meaningless. Another important step before pose selection is rank determination, by employing the SVD to eliminate poorly identifiable parameters.

2 Observability Indices

Assume the robot is placed into p poses. Following the formulation in [5, 6, 13], all kinematic calibration methods are considered as closed-loop methods, wherein any endpoint measurement system is considered to form a joint. Consequently, form the kinematic loop closure equations for the ith pose ($i = 1, ..., p$):

$$\mathbf{f}^i = \mathbf{g}^i(\mathbf{x}, \mathbf{v}^i) \approx 0 \tag{1}$$

where $\mathbf{f}^i$ is a residual function due to the inaccuracy of the kinematic parameters, sensor noise, and unmodeled errors, $\mathbf{g}^i$ is the loop closure equation, $\mathbf{x}$ is a vector of robot parameters to be calibrated, and $\mathbf{v}^i$ is a vector of joint sensor readings and possibly external sensor readings. Combine (1) for the p poses into a single matrix equation:

$$\mathbf{f} = \mathbf{g}(\mathbf{x}) \tag{2}$$

where $\mathbf{f} = [\mathbf{f}^{1T} \ldots \mathbf{f}^{pT}]^T$ and $\mathbf{g} = [\mathbf{g}^{1T} \ldots \mathbf{g}^{pT}]^T$. In (2), we treat the sensor readings $\mathbf{v}^i$ as constants for each pose i. Linearize (2) around the nominal values of the parameters:

$$\Delta\mathbf{f} = \frac{\partial \mathbf{g}}{\partial \mathbf{x}} \Delta\mathbf{x} = \mathbf{C}\Delta\mathbf{x} \tag{3}$$

where $\Delta\mathbf{f}$ is the error between measured and computed residual function, $\mathbf{C}$ is the identification Jacobian, and $\Delta\mathbf{x}$ is the correction to be applied to the current parameter estimate. The calibration problem is then solved by minimizing $\Delta\mathbf{f}$ via iterative least squares. Define the SVD of the identification Jacobian in (3):

$$\Delta\mathbf{f} = \mathbf{C}\Delta\mathbf{x} = \mathbf{U}\boldsymbol{\Sigma}\mathbf{V}^T\Delta\mathbf{x} \tag{4}$$

0-7803-2988-4/96 $4.00

where $\mathbf{U}$ and $\mathbf{V}$ are orthogonal matrices and $\mathbf{\Sigma}$ is a matrix which is made up of the singular values of $\mathbf{C}$ in its main diagonal and zero for other elements. If we assume that at each pose, q equations (for position and orientation) are used, the robot is placed into p positions, and there are L parameters after rank determination, then $\Delta\mathbf{f}$ will be a $q.p$-vector, $\mathbf{C}$ a $q.p \times L$ matrix, $\Delta\mathbf{x}$ an L-vector, $\mathbf{U}$ a $q.p \times q.p$ matrix, $\mathbf{V}$ an $L \times L$ matrix, and

$$\mathbf{\Sigma} = \begin{bmatrix} \mathbf{S} \\ \mathbf{O}_{q.p-L,L} \end{bmatrix}$$

where $\mathbf{S} = diag(\sigma_1, ..., \sigma_L)$ is the matrix of ordered singular values. To avoid an underdetermined system of equations, $q.p$ should be at least equal to L. *Again, we emphasize that parameter and task variable scalings should be implemented before comparing singular values.*

In this paper, we assume output noise only: the sensor noise affects $\mathbf{f}$ and has little influence on the identification Jacobian $\mathbf{C}$. In case of input noise, one possibility is to augment the standard deviations of output noise by scaled versions of the input noise standard deviations before performing task variable scaling [14]. However, we are leaving this issue for future research. Next, we consider 3 published observability indices before introducing the noise amplification index.

2.1 The Product of Singular Values

Borm and Menq [2, 8] selected the geometric mean of all the singular values as the observability index, which we will label O_1:

$$O_1 = \frac{\sqrt[L]{\sigma_1 ... \sigma_L}}{\sqrt{m}} \tag{5}$$

where m is the number of poses. This index is related to the determinant of $\mathbf{C}^T\mathbf{C}$:

$$\sqrt{det(\mathbf{C}^T\mathbf{C})} = \sigma_1 ... \sigma_L \tag{6}$$

The rationale derives from the following basic relationship [8]:

$$\sigma_L \leq \frac{|| \Delta\mathbf{f} ||}{|| \Delta\mathbf{x} ||} \leq \sigma_1 \tag{7}$$

where σ_L is the smallest singular value of $\mathbf{C}$ and σ_1 is the largest one. It is desired that a very small change in parameters, $\Delta\mathbf{x}$, makes the largest possible effect on the residual error function $\Delta\mathbf{f}$. Thus we wish to make $|| \Delta\mathbf{f} || / || \Delta\mathbf{x} ||$ as big as possible.

From a geometrical viewpoint, if we assume that $\Delta\mathbf{x}$ defines a hypersphere with a unit radius, then $\Delta\mathbf{f}$

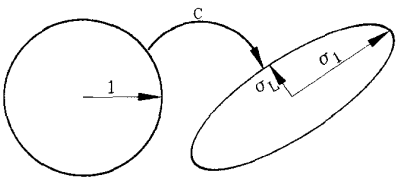

Figure 1: Geometric interpretation of singular values.

is a hyperellipsoid whose semiaxes are the singular values of the gradient matrix $\mathbf{C}$ (Figure 1). Modifying results in the mathematics literature, we can show that the volume V_L of this hyperellipsoid is proportional to the product of the singular values of $\mathbf{C}$:

$$V_L = \frac{2\pi^{L/2} \prod_{i=1}^{L} \sigma_i}{L.\Gamma(L/2)} \tag{8}$$

The geometric rationale behind the observability index O_1 is to make the volume of this hyperellipsoid as big as possible. This means that a parameter error vector results in a good *aggregate* increase in the measurable vector $\Delta\mathbf{f}$. The disadvantage of this index is that we cannot guarantee the $\Delta\mathbf{f}$ vector is necessarily large in a voluminous hyperellipsoid. Imagine a big hyperellipsoid whose axes are all large except one. If we are unlucky, the $\Delta\mathbf{f}$ vector may be as small as the small semi-axis.

2.2 The Inverse Condition Number

Driels and Pathre [3] suggested the condition number of $\mathbf{C}$ as observability index. To accord with other observability indices which should be maximized, we use the inverse condition number O_2, whose maximum value is 1:

$$O_2 = \frac{\sigma_L}{\sigma_1} \tag{9}$$

They also stated that the reduction in the range of motion of a joint during calibration implies less observability of the parameters of that joint, and this is accompanied by an order of magnitude increase in the condition number.

Due to noise from the sensors or unwanted error sources ($\delta\Delta\mathbf{f}$), $\Delta\mathbf{x}$ in (4) has an error $\delta\Delta\mathbf{x}$. (Remember that $\Delta\mathbf{x}$ results from the difference between the actual and the nominal values of the parameters.) Strang gives [12]:

$$\frac{|| \delta\Delta\mathbf{x} ||}{|| \Delta\mathbf{x} ||} \leq \frac{\sigma_1}{\sigma_L} \frac{|| \delta\Delta\mathbf{f} ||}{|| \Delta\mathbf{f} ||} \tag{10}$$

To minimize the error of the estimated parameters $|| \delta\Delta\mathbf{x} ||$, we should make σ_1/σ_L as small as possi-

ble, i.e., O_2. Geometrically, this ratio is a measure of the eccentricity of the hyperellipsoid of $\Delta\mathbf{f}$. A bigger O_2 makes the hyperellipsoid closer to a hyper-sphere. This measure does not consider the size of the hyperellipsoid, but rather its eccentricity. An advantage of this index is that it is dimensionless, because of the ratio of two singular values.

2.3 The Minimum Singular Value

The first inequality of (7) is rewritten as:

$$|| \Delta\mathbf{f} || \geq \sigma_L || \Delta\mathbf{x} || \tag{11}$$

i.e., the greater the minimum singular value of $\mathbf{C}$, the greater $|| \Delta\mathbf{f} ||$. Thus define the observability index :

$$O_3 = \sigma_L \tag{12}$$

O_3 conveys the idea that the residual error function $|| \Delta\mathbf{f} ||$ is maximally related to the error of parameters from their nominal values. Geometrically, this observability index requires a large minimum axis of the hyperellipsoid $\Delta\mathbf{f}$.

2.4 The Noise Amplification Index

To summarize from the geometrical point of view, O_1 is related to the lengths of all semiaxes, O_2 to the lengths of the shortest and largest semiaxes, and O_3 to the length of the shortest semi-axis.

Equation (10) is important. It says that if we wish a low value for $|| \delta\Delta\mathbf{x} || / || \Delta\mathbf{x} ||$, we should minimize both σ_1/σ_L and $1/|| \Delta\mathbf{f} ||$. The minimization of σ_1/σ_L is achieved by a large O_2 and the minimization of $1/|| \Delta\mathbf{f} ||$ is achieved by a large O_3.

To clarify that O_2 or O_3 cannot be used alone, assume a hypothetical robot with three parameters which is calibrated by two pose sets A and B. For pose sets A and B, suppose the singular values are:

$$\boldsymbol{\sigma}^A = [100, 0.1, 0.1] \tag{13}$$

$$\boldsymbol{\sigma}^B = [10, 10, 0.01] \tag{14}$$

Both pose sets have the same O_1 index. The minimum singular value O_3 suggests that pose set A yields better observability, while the inverse condition number O_2 treats them the same. This example shows the defect of the inverse condition number O_2 : it does not consider the absolute value of σ_3.

Consider a third hypothetical pose set C with singular values:

$$\boldsymbol{\sigma}^C = [10, 1, 0.1] \tag{15}$$

Compared to pose set A, the σ_1's are different, but the σ_3's are the same. In this case, the inverse condition number O_2 prefers pose set C to pose set A, but the minimum singular value O_3 treats them the same. This lack of discrimination regarding the largest singular value is the defect of the minimum singular value O_3.

We also note that the volume of the hyperellipsoid cannot be a good indication of the observability because it is not based on the worst case design criterion. Equation (11) tells us that as long as we have a small minimum singular value, we may have trouble in having a big and measurable $\Delta\mathbf{f}$.

We now combine the inverse condition number O_2 and the minimum singular value O_3 to overcome the disadvantages of each:

$$O_4 = \frac{\sigma_L}{\sigma_1}\sigma_L = \frac{\sigma_L^2}{\sigma_1} \tag{16}$$

The larger this index, the better the observability and accuracy of the calibration procedure. We name it the *noise amplification index,* because we will shortly show that it is an indicator of the amplification of the sensor noise and unmodeled errors.

For the previous example, O_4 is equal to 10^{-4} for pose set A and 10^{-5} for pose set B, and hence selects pose set A over pose set B. This is an advantage over O_2 which does not take into account the minimum singular value. For pose set C, O_4 is equal to 10^{-3}, and hence selects pose set C over pose set A. The noise amplification index O_4 takes into account the condition number, which is an advantage over the minimum singular value O_3.

The following theorem provides a formal rationale for the noise amplification index O_4 .

Theorem 1 *If $\delta\Delta\mathbf{f}$ denotes the error of the residual error function due to sensor noise or unmodeled errors in a robot calibration pose set, the maximum amplification factor of the corresponding error in the identified parameters is σ_1/σ_L^2.*

Proof. Replace $\Delta\mathbf{f}$ in (10) by its minimum value from (11). Equation (10) still holds:

$$\frac{|| \delta\Delta\mathbf{x} ||}{|| \Delta\mathbf{x} ||} \leq \frac{\sigma_1}{\sigma_L}\frac{|| \delta\Delta\mathbf{f} ||}{\sigma_L || \Delta\mathbf{x} ||} \tag{17}$$

or:

$$|| \delta\Delta\mathbf{x} || \leq \frac{\sigma_1}{\sigma_L^2} || \delta\Delta\mathbf{f} || \tag{18}$$

Equation (18) clearly shows that the unwanted error of the calibrated parameters, $|| \delta\Delta\mathbf{x} ||$, is an amplification of the residual error function noise, $|| \delta\Delta\mathbf{f} ||$, by a factor of σ_1/σ_L^2. Hence the formal rationale for the noise amplification index O_4 : the bigger O_4, the smaller σ_1/σ_L^2, and the smaller $|| \delta\Delta\mathbf{x} ||$. Geometrically, O_4 conveys the requirement for a hyperellipsoid which has a large minimum axis and is only mildly eccentric.

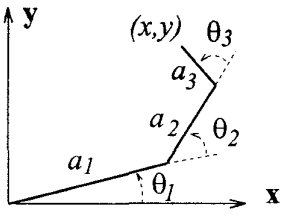

Figure 2: A 3-link planar robot.

3 Results

In this section, we present two kinematic calibration studies to evaluate the four observability indices . The first study is a simulation of a 3-link planar robot, and the second study is a simulation plus experiment for a 3-DOF redundant parallel-drive robot.

3.1 A 3-Link Planar Robot

Figure 2 shows the simulated 3-link planar robot. The end point position (x, y) is expressed in coordinate zero. We suppose it is tracked by an external measuring device with an RMS error of 3 mm normally distributed. (This is roughly the performance of magnetic trackers, although the exact accuracy is not important here.) Joint angle errors are assumed negligible.

3.1.1 Calibration Procedure

We form a residual error function $\mathbf{f}$ and minimize it:

$$\begin{aligned} f(2k-1) &= a_1 cos(\theta_1(k)) + a_2 cos(\theta_1(k) + \theta_2(k)) \\ &\quad + a_3 cos(\theta_1(k) + \theta_2(k) + \theta_3(k)) - x(k) \\ f(2k) &= a_1 sin(\theta_1(k)) + a_2 sin(\theta_1(k) + \theta_2(k)) \\ &\quad + a_3 sin(\theta_1(k) + \theta_2(k) + \theta_3(k)) - y(k) \end{aligned}$$

where $k = 1, ..., p$ is the pose number. Angle $\theta_i(k), i = 1, 2, 3$ is obtained by:

$$\theta_i(k) = s_i * v_i(k) + \theta_{0i} \tag{19}$$

where s_i, $v_i(k)$, and θ_{0i} represent the gain, sensor reading, and offset of joint i respectively. Thus, we have 9 parameters to calibrate: $a_i, s_i, \theta_{0i}, i = 1, 2, 3$. Nominal values for link lengths a_i's are 2000, 1000, 500 mm, for all gains $\pi/20$ rad/v, and for offsets $\pi/6$, $\pi/3$, $\pi/2$ rad. Sensor reading range is $[-10, +10]v$. The Jacobian $\mathbf{C}$ can be easily determined using the residual error equations.

3.1.2 Simulation Results

Using Matlab^{TM}, we generated 343 equally spaced poses using the selected robot parameters. To the resulting x, y endpoint coordinates was added a normally distributed noise level of 3 mm. These noise-corrupted x, y values were used as input to a calibration routine to determine the 9 parameters mentioned in the previous section. Column scaling which is a type of parameter scaling was performed before evaluating indices [6]. We do not need to perform task variable scaling since x and y have the same unit and uncertainty. Each time we ran the calibration routine, 50 poses from 343 poses were selected randomly as a pose set.

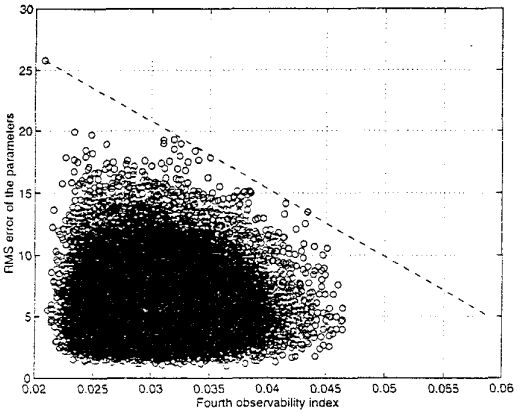

Figure 3: Noise amplification index O_4 versus the RMS error of the scaled parameters.

Figure 3 shows the results of running the calibration routine 50,000 times. Each circle shows the result of one pose set (50 poses). It is seen how the upper limit (dashed line) of the RMS error of the scaled parameters decreases while the noise amplification index O_4 increases. The RMS error is the difference between the results of calibration routine and the true values of the 9 parameters. For example, when O_4 is 0.021, the upper limit of the RMS error of the scaled parameters is 25.8. When O_4 increases to 0.043, the error is not greater than 14.

Similarly, the relation of the RMS error of the parameters with other observability indices is shown in Figure 4. In order to compare these indices, we scaled them so that the minimum value of each index is 1. Again, the upper limits are shown by dashed lines. Looking at the range of change of each index, we realize the sensitivity of these indices are quite different from each other. Figure 5 shows the upper limit lines. It is easily computed that the noise amplification index O_4 is 94% more sensitive to the RMS error of the parameters than the minimum singular value O_3, 273% more sensitive than the inverse condition num-

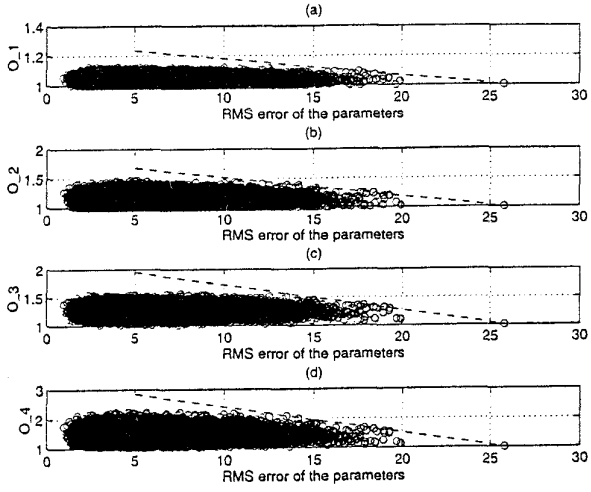

Figure 4: Scaled observability indices versus the RMS error of the parameters.

ber O_2, and 785% more sensitive than the product of singular values index O_1. This greater sensitivity is a clear advantage of the noise amplification index O_4 over the other indices.

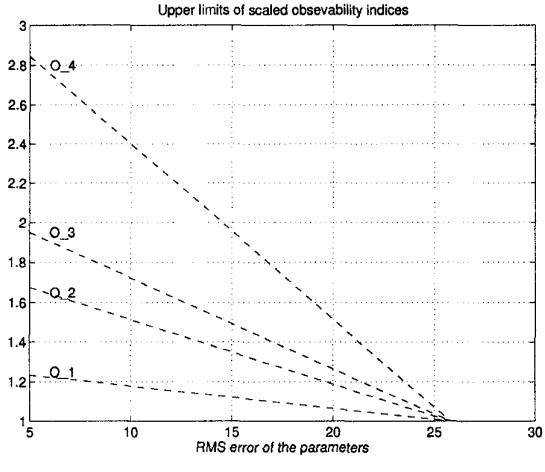

Figure 5: Comparison of the sensitivity of the observability indices to the RMS error of the parameters.

We are also interested in the relation among these indices. Figure 6 shows how the first three indices change versus the noise amplification index O_4. In Figure (a), there is no clear relation between the noise amplification index O_4 and index O_1. In Figure (b), there is an almost linear relationship between the noise amplification index O_4 and the inverse condition number O_2, though near small values of O_4, this relation

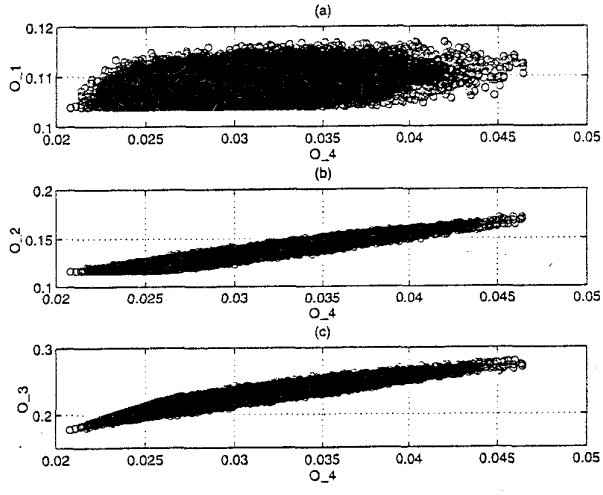

Figure 6: Comparison of the the first three observability indices to the noise amplification index O_4.

almost vanishes. Finally, in Figure (c), as the noise amplification index O_4 increases, the minimum singular value O_3 increases almost linearly. If we want to find O_4 using a linear approximation in each of the three figures, maximum errors as much as 0.016 in Figure (a), 0.004 in Figure (b), and 0.005 in Figure (c) will result. Considering the overall range of O_4, these maximum errors are not negligible. Thus, we conclude that knowing each of the first three indices does not give us an accurate O_4.

3.2 Redundant Parallel-Drive Robot

This mechanism is a 3-DOF platform type closed-chain mechanism with its output link constrained to undergo spherical motions (Figure 7) [4]. In Figure 7, d_i (i=1,2,3,4) is the input of the mechanism and represents a pair of actuator and displacement sensor. $\mathbf{A}_i$ (i=1,2,3,4) represents a spherical joint at the stationary side of each actuator. $\mathbf{B}_1$ and $\mathbf{B}_2$ are universal joints and lie in the intersection of the centerlines of each two adjacent actuators. Plane $\mathbf{B}_1\mathbf{B}_2\mathbf{O}$ defines the end plate which should be placed into the desired orientation. k_1 and k_2 are imaginary links used in calibration loops.

3.2.1 Calibration Procedure

The kinematic loop formulations [6] requires measurement of all joint angles. Since the angles are not sensed in this mechanism, the simplest way to formulate calibration equations is to use distance equations. We use measurement redundancy to establish our objective function which is to be minimized. Assume we

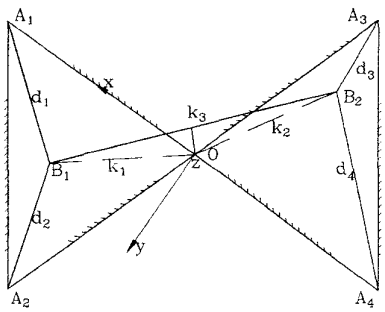

Figure 7: Kinematic model of the shoulder joint viewed from above.

move the mechanism into p different poses. Define the error vector $\mathbf{f}$ with the following components:

$$f(k) = (\mathbf{B}_1(k) - \mathbf{B}_2(k))^2 - k_3^2 \qquad (20)$$

where $k = 1, ..., p$ represents the pose number. $\mathbf{B}_1(k)$ and $\mathbf{B}_2(k)$ are the position vectors of the end plate universal joints in the k'th pose [10]. Length $d_i(k)$ which is measured by the i'th LVDT in the k'th pose is obtained as follows:

$$d_i(k) = s_i * v_i(k) + d_{0i} \, (i = 1, ..., 4, k = 1, ..., p) \quad (21)$$

where s_i, $v_i(k)$, and d_{0i} represent the gain, output voltage, and offset of the i'th LVDT respectively. It is worth mentioning that each time LVDT's are disassembled and then reassembled, d_{0i} may change considerably (a few millimeters) and the closed-loop calibration is a promising approach for finding new offsets.

The objective function and solution procedure were outlined in Section 2.

3.2.2 Simulation Results

Figure 8 gives the simulation results for several pose sets selected randomly from 280 poses. Each pose set includes 30 poses. The RMS error between the true values of parameters and those obtained by the routine is shown versus the four observability indices. A noise level of 4 mv (10% of the real noise level) was assumed for the LVDT's for faster convergence of the optimization. Column scaling (a type of parameter scaling) was performed in order to make singular values comparable.

It is seen that O_1 gives poor results. Specifically, there are two coincident pose sets which have the worst RMS error in spite of a large O_1. In the figure of the inverse condition number O_2 all the points are below a limit curve (dashed line); as O_2 increases, the upper limit of the RMS error decreases. This curve was

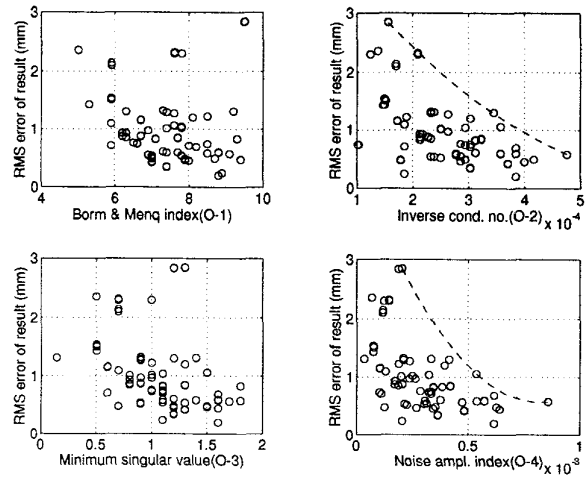

Figure 8: Comparison of the observability indices for a sensor noise of 4mv.

fitted in such a way that all the points lie under the curve. The minimum singular value O_3 gives a better indication than index O_1. For large values of O_3, the RMS error is small, but still for O_3=1.3 and 1.2, we see poor results of more than 2.5 mm RMS error. The noise amplification index O_4 gives an upper limit curve similar to that of O_2, In summary, simulation results show that O_1 is a poor indication of observability, and that the minimum singular value O_3 cannot be used alone. The inverse condition number O_2 and the noise amplification index O_4 gave good results.

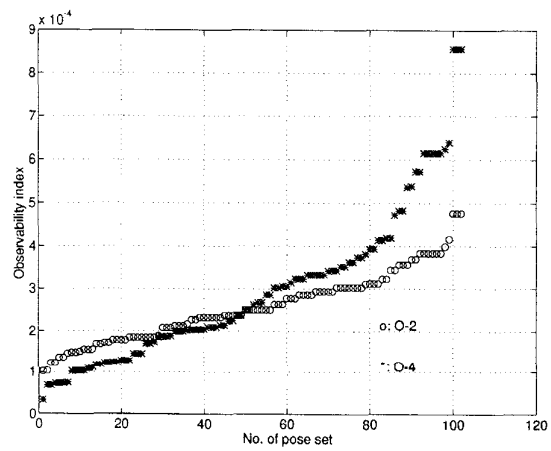

Figure 9: Comparison of the sensitivity of observability indices O_2 and O_4 with a sensor noise of 4mv.

Figure 9 compares the inverse condition number O_2 and the noise amplification index O_4, for more than 100 pose sets obtained in the noise simulation re-

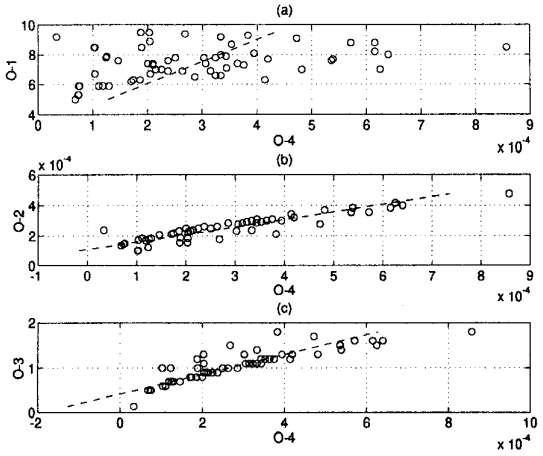

Figure 10: Variation of observability indices O_1, O_2, and O_3 versus O_4. Dashed lines represent linear approximations.

sults. The inverse condition number O_2 changes from 1.02×10^{-4} to 4.76×10^{-4} while the noise amplification index O_4 changes from 0.33×10^{-4} to 8.57×10^{-4}. The noise amplification index O_4 is 2.2 times more sensitive, and confirms its advantage over the inverse condition number O_2.

Figure 10 shows the first three indices versus O_4. Dashed lines represent linear fittings. In Figure (a), it is easily seen that there is no good correspondence between O_4 and O_1. The maximum error between the computed O_4 and fitted line is 4.9×10^{-4} which is quite big. In Figure (b), there is an almost linear correspondence between O_4 and O_2. The maximum error between the computed O_4 and fitted line is 2.2×10^{-4}. There is a rough linear relation between O_4 and O_3 in Figure (c) for small values of O_4, but at large values this relation vanishes. For example, at $O_3 \approx 2$, O_4 can be between 4×10^{-4} and 9×10^{-4}. The maximum error between the computed O_4 and fitted line is 2.5×10^{-4}. We conclude from these three figures that we cannot necessarily predict observability index O_4 from observability indices O_1, O_2, and O_3.

Note that in Figure 8, we have very accurate results for some pose sets in spite of small observability indices. This is always the case because the role of the observability index is only to guarantee a small RMS error in the presence of large values of observability index. For small observability indices, the results are chaotic: sometimes accurate and sometimes poor. In other words, an observability index gives us an upper limit for the error and not a lower limit.

Parameter	Initial guess	Calibration results			
		$O_4 < .00025$		$O_4 > .00081$	
		Typ. result	Stand. dev.	Typ. result	Stand. dev.
d_{01}	95.0	99.1	0.8	97.8	0.4
d_{02}	95.0	98.0	1.1	99.3	0.8
d_{03}	95.0	97.7	1.2	96.2	0.8
d_{04}	95.0	97.0	0.8	100.4	0.4
s_1	3.60	3.605	0.058	3.664	0.036
s_2	3.60	3.697	0.040	3.631	0.014
s_3	3.60	3.538	0.026	3.581	0.011
s_4	3.60	3.733	0.042	3.670	0.026

Table 1: Experimental results of calibrating the redundant parallel-drive robot. Offsets are in *mm* and gains are in mm/v.

3.2.3 Experimental Results

The end plate was moved into different orientations manually and data were acquired simultaneously from four LVDT's through 12-bit A/D converters with a sampling frequency of 20 Hz. 450 poses were recorded. We wrote an algorithm in Matlab^{TM} to select 50 poses out of 450 poses and recorded the final results along with observability indices. This procedure of random pose selection was repeated for 150 times.

Table 1 shows typical results for two extreme cases: low and high values for the noise amplification index O_4. We recorded the results of 5 pose sets where $O_4 < 0.00025$ and 5 pose sets where $O_4 > 0.00081$. We then calculated the standard deviation of the results of these 5 pose sets for each parameter. From Table 1, one can easily compute that the standard deviations of results for pose sets with high values of O_4 are between 34% and 77% of the standard deviation for the low O_4 case. This complies with our expectation that the calibration results will be more robust if we have high values of O_4.

4 Discussion

We have presented the noise amplification index as a new observability index to find the best pose set of a robot in the kinematic loop calibration methods. The proposed index was analyzed analytically and geometrically, in comparison to three previously proposed indices. Simulation and experimental results confirmed the effectiveness of the new index.

In our method, we first created several poses in the simulation and then selected several pose sets out of these created poses. The optimum pose set was the one with the biggest observability index. This would

be a cumbersome task if we had more DOF's. To overcome the difficulty of checking the observability index for all the possible pose sets, Zhuang et al. [15] proposed a simulated annealing approach to obtain optimal measurement pose set for robot calibration. They defined an observability index, e.g. condition number, as a cost function and minimized it through the simulated annealing optimization algorithm. They stated that this method can escape local minimum points.

For those cases where noise perturbs the identification Jacobian, one should consider more complex measures. This is a research area which needs more work. For example, we might get better pose sets for the redundant parallel-drive robot if we consider perturbation of the identification Jacobian too.

While this paper has emphasized kinematic calibration, the results are generally pertinent to any robot calibration problem, such as estimation of inertial parameters [1]. Finally, we believe that the ideas of this paper can be used in their parallel for dexterity measures of redundant manipulators. The first three observability indices have been already proposed as dexterity measures [10]. We are interested to develop a manipulability similar to the noise amplification index O_4.

Acknowledgments

Support for this research was provided by the NSERC NCE IRIS II Project AMD-5, and by NSF Grant MIP-9508588.

References

[1] Armstrong, B., "On finding exciting trajectories for identification experiments involving systems with nonlinear dynamics," *Int. J. Robotics Research*, vol. 8, no. 6, pp. 28-48, 1989.

[2] Borm, J.H., and Menq, C.H., "Determination of optimal measurement configurations for robot calibration based on observability measure," *Intl. J. Robotics Research*, vol. 10.1, pp. 51-63, 1991.

[3] Driels, M.R., and Pathre, U.S., "Significance of observation strategy on the design of robot calibration experiments," *J. of Robotic Systems*, vol. 7, no. 2, pp. 197-223, 1990.

[4] Hayward, V., "Design of a hydraulic robot shoulder mechanism based on a combinatorial mechanism," *Preprints of the Third Int. Symposium on Experimental Robotics*. Kyoto, Japan:, 1993.

[5] Hollerbach, J.M., "Advances in robot calibration," in *Robotics Research: The Sixth International Symposium*, Hidden Valley, PA, pp. 319-326, Oct. 2-5, 1993.

[6] Hollerbach, J.M., and Wampler, C.W., "The calibration index and taxonomy for robot kinematic calibration methods," *Intl. J. Robotics Research*, 1996, in press.

[7] Klein, C.A., and Blaho, B.E., "Dexterity measures for the design and control of kinematically redundant manipulators," *Intl. J. Robotics Research*, vol. 6, no. 2, pp. 72-83, 1987.

[8] Menq, C.H., Borm, J.H., and Lai, J.Z., "Identification and observability measure of a basis set of error parameters in robot calibration," *J. Mechanisms, Transmissions, and Automation in Design*, vol. 111, pp. 513-518, 1989.

[9] Mooring, B.W., Roth, Z.S., and Driels, M.R., *Fundamentals of Manipulator Calibration*. NY: Wiley Interscience, 1991.

[10] Nahvi, A., Hollerbach, J.M., and Hayward, V., "Calibration of a parallel robot using multiple kinematic closed loops," *Proc. IEEE Intl. Conf. Robotics and Automation*, pp. 407-412, 1994.

[11] Schroer, K., "Theory of kinematic modelling and numerical procedures for robot calibration," *Robot Calibration*, edited by R. Bernhardt et al.. London: Chapman & Hall, pp. 157-196, 1993.

[12] Strang, G., *Linear Algebra and its Applications*. New York: Academic Press, 1980.

[13] Wampler, C.W., Hollerbach, J.M., and Arai, T., "An Implicit Loop Method for kinematic calibration and its application to closed-chain mechanisms," *IEEE Trans. Robotics and Automation*, vol. 11, 1995, in press.

[14] Zak, G., Benhabib, B., Fenton, R.G., and Saban, I., "Application of the weighted least squares parameter estimation method for robot calibration," *J. Mechanical Design*, vol. 116, pp. 890-893, 1994.

[15] Zhuang, H., Wang, K., and Roth, Z.S., "Optimal selection of measurement configurations for robot calibration using simulated annealing," *Proc. IEEE Intl. Conf. Robotics and Automation*, pp. 393-398, 1994.